frontiers | Frontiers in Earth Science

TYPE Original Research
PUBLISHED 07 November 2024
DOI 10.3389/feart.2024.1367771

Check for updates

OPEN ACCESS

EDITED BY
Petra Heil,
Australian Antarctic Division, Australia

REVIEWED BY
Hongbo Li,
Ningxia University, China
Jiaxing Jiaxing,
Chengdu University of Technology, China

*CORRESPONDENCE
Zhilong Zhang,
zhangzl@xju.edu.cn

RECEIVED 09 January 2024
ACCEPTED 07 October 2024
PUBLISHED 07 November 2024

CITATION
Bao D, Zhang Z, Yue Z, Zhang A and Liu G (2024) Study on the water–salt migration law of salinized frozen soil based on the capillary model.
Front. Earth Sci. 12:1367771.
doi: 10.3389/feart.2024.1367771

COPYRIGHT
© 2024 Bao, Zhang, Yue, Zhang and Liu. This is an open-access article distributed under the terms of the Creative Commons Attribution License (CC BY). The use, distribution or reproduction in other forums is permitted, provided the original author(s) and the copyright owner(s) are credited and that the original publication in this journal is cited, in accordance with accepted academic practice. No use, distribution or reproduction is permitted which does not comply with these terms.

Study on the water–salt migration law of salinized frozen soil based on the capillary model

Dejun Bao[1], Zhilong Zhang[2]*, Zheng Yue[2], Ao Zhang[2] and Guang Liu[2]

[1]Gansu Zhonghai Security Technology Co., Ltd., Lanzhou, China, [2]College of Civil Engineering and Architecture, Xinjiang University, Urumqi, China

Salt expansion and frost heave are the main diseases of salted frozen soil roadbeds. Salt swelling and frost heave disease are closely related to the salted soil water–salt migration, temperature variation, and salt crystallization amount change. This article establishes a coupled model of water, heat, and salt fields based on the capillary model and the unfrozen water characteristic curve. The study shows that the different initial moisture contents have minimal effects on the location of soil salt migration and aggregation. The different initial salt concentrations have a substantial effect on the soil water–salt migration aggregation position; when the concentration of sodium sulfate increases, different from chloride saline soils, the position of the freezing front fluctuates up and down over time. The water–salt migration and aggregation are smaller in the closed condition, where they are reduced by 38% and 20%, respectively.

KEYWORDS

salinized frozen soil, hydrothermal salt coupling, water–salt migration, crystallization, temperature variation

1 Introduction

Salinized frozen soil has the dual nature of ordinary salinized soil and frozen soil (Xiao et al., 2018; Davidson et al., 1969). Under the action of external temperature, the pore water repeatedly freezes and melts to cause soil freezing and thawing as well as sinking, and the salts in the pore water repeatedly crystallize and dissolve to cause soil salinization and dissolution sinking, resulting in the double disease of salinization as well as freezing and thawing of engineering facilities constructed on salinized frozen soil (Xiao and Lai, 2018; Niu and Gao, 2015).

The pore water in the soil migrates from the warm to the cold section under unidirectional freezing conditions and aggregates in the freezing fronts, which produces a significant freezing expansion (Gardner, 1958; Zhang et al., 2016). Therefore, frost heave damage in soils is due to water migration. Salt swelling occurs in saline soils due to the crystallization of soluble salts in the soil mass (Huang et al., 2008; Bing and Ma, 2011). In an area of sulfate-salted soil, the solubility of sulfate decreases with temperature, and the sulfate in the soil crystallizes and precipitates, demonstrating a 3.18× volume increase.

Water–salt migration is the leading factor in salt swelling (dissolution subsidence) and frost swelling (thawing and sinking) (Bing et al., 2015; Spaans and Baker, 1996). The current water-blocking measures for saline soil roadbeds in Xinjiang, which are based on coarse-grained filler layers or an additional insulating layer, have already achieved a certain effect in the management of saline frozen soil roadbed diseases (Peng et al., 2023;

Peng et al., 2021). However, after the seasonal freezing and thawing, monitoring results indicated that in the upper layer of the constructed roadbed, the water content doubled in winter compared to summer, and the accumulation of salts increased by more than 10 times (Wang et al., 2019; Watanabe and Flury, 2008). This finding indicates that the water barrier measures taken only hindered the upward migration rate of water but did not insulate it. In the winter process of moisture migration to the freezing front, the formation of sub-condensation ice, frost expansion, salt with moisture migration aggregation, insulation layer corrosion, and the occurrence of salt expansion contributed to the failure of the related disease prevention measures (Lai et al., 2021; Zhang et al., 2021a).

The capillary model is an important method of studying water migration in soil. The study introduces a hydraulic conductivity model for frozen soils, accounting for water films. It partitions water in capillary tubes into free water and water films with varying dynamic viscosities (Ming et al., 2022). Based on the discontinuous noncircular capillary bundle model, it predicts the hydraulic conductivity of warm, saturated frozen soil, primarily determined by the unfrozen water content, regulated by temperature and soil particle size distribution (Chai et al., 2018). The study concludes that before freezing, NaCl does not crystallize and has minimal impact on the permeability coefficient. However, Na_2SO_4 crystallizes, blocking pores and reducing the permeability coefficient as temperature decreases. The freezing temperature significantly impacts the permeability coefficient (Liu et al., 2023; Zhang and Guan, 2022).

Researchers developed various models to understand the mechanisms and control of salt expansion. One model, validated by uniaxial freezing tests, focuses on the hydro-thermal-salt-mechanical coupling in saturated and unsaturated salinized soil under unidirectional freezing (Wang et al., 2016). The model introduced the concept of an uncrystallized zone, positively related to the cold-end temperature. Considering sodium sulfate crystallization, it predicts the coupled transfer of water, heat, and solute in saline loess (Xu et al., 2021). The study corrected the hydrothermal salt force coupled equations for coarse-grained sulfate saline soil roadbeds, providing insights into the water and salt migration mechanism in the roadbed (Zhang et al., 2020).

In conclusion, the driving force and permeability coefficient are key parameters in the water–salt migration model of salinized frozen soil. Therefore, this paper uses the capillary model and the unfrozen water characteristic curve to study the water–salt migration law of salinized positive frozen soil.

2 Materials and methods

2.1 Temperature field control equations

Conduction, radiation, and convection are the three main modes of heat transfer. Heat conduction is the main mode of heat transfer in salinized frozen soil in nature, and the effects of convection and radiation can be neglected (Luo et al., 2023; He et al., 2021). Assuming that the salinized frozen soil is an isotropic continuous medium, unfrozen water, crystalline salt, soil particles, and ice crystals are incompressible. Ignoring convective heat due to moisture seepage, according to Fourier's law of heat conduction and the law of energy conservation, the crystallization of moisture salts will release heat (Wang et al., 2016; Zhang et al., 2020). Treating the phase changes of water and salt crystallization as heat sources, the differential equation of heat conduction in salinized frozen soil is Equation 1 (Deng et al., 2021):

$$\rho C(\theta)\frac{\partial T}{\partial t} = \lambda(\theta)\nabla^2 T + L_c\frac{\partial \theta_c}{\partial t} + L_i\rho_i\frac{\partial \theta_i}{\partial t}, \tag{1}$$

where ∇ is the Hamiltonian operator for two-dimensional $[\partial/\partial x, \partial/\partial y]$; T is the temperature of the soil; t is the time; L_c and L_i are the latent heat of phase change of crystalline salt and ice; ρ_c and ρ_i are the densities of the crystalline salt and ice, respectively; θ_c and θ_i are the volume contents of the crystalline salt and the pore ice, respectively; λ is the thermal conductivity unit of W/(m-K), which is expressed by the following Equations 2, 3:

$$\lambda(\theta) = \lambda_s^{\theta_s}\lambda_i^{\theta_i}\lambda_c^{\theta_c}\lambda_u^{\theta_u}, \tag{2}$$

where λ_s is the thermal conductivity of soil; λ_i is the thermal conductivity of ice; λ_c is the thermal conductivity of crystalline salt; λ_u is the thermal conductivity of water; θ_s, θ_i, θ_c, θ_u, are the proportions of the corresponding substances; C is the specific heat capacity, which can be expressed by the sum of the components of the volume-specific heat capacity:

$$\rho C(\theta) = \rho_s C_s\theta_s + \rho_i C_i\theta_i + \rho_c C_c\theta_c + \rho_w C_u\theta_u, \tag{3}$$

where C_s is the specific heat capacity of the earth; C_i is the specific heat capacity of ice; C_c is the specific heat capacity of crystalline salt; C_u is the specific heat capacity of water.

2.2 Equation of control for the moisture field

Unfrozen water always exists in the frozen soil. The migration of water follows Darcy's law (Ming et al., 2022; Andersland et al., 1996). According to Richard's Equation 4 (Chai et al., 2018; Burt and Williams, 1976), the total water content of saline soil comprises three components: ice, unfrozen water, and mannite crystalline water:

$$\theta_T = \theta_u + \frac{\rho_i}{\rho_w}\theta_i + \frac{\rho_c M_{180}}{\rho_w M_c}\theta_c, \tag{4}$$

where θ_T the total water content, M_c is the molecular mass of the crystalline salt; M_{180} is the molecular mass of the bound water in the crystalline salt.

The ratio of ice to unfrozen water volume content as a function of temperature with temperature reduction is as follows (Bai et al., 2015; Watanabe and Osada, 2016) (Equation 5):

$$B_i = \frac{\theta_i}{\theta_u}\begin{cases} 1.1\left(\frac{T}{T_i}\right)^B - 1 & (T < T_i) \\ 0 & (T \geq T_i), \end{cases} \tag{5}$$

where B is a constant related to the type of soil and salt content. The values of 0.61, 0.47, and 0.56 are taken for sandy, pulverized, and clay soils, respectively, and T_i is the freezing temperature.

The differential equation for water infiltration in salted frozen soil is Equation 6

$$\frac{\partial \theta_u}{\partial t} + \frac{\rho_i}{\rho_w}\frac{\partial \theta_i}{\partial t} + \frac{\rho_c M_{180}}{\rho_w M_c}\frac{\partial \theta_c}{\partial t} = \nabla\left[D(\theta_u)\nabla\theta + k_g(\theta_u)\right], \tag{6}$$

where θ_u is the volume content of unfrozen water in the frozen soil; k_g is the permeability coefficient of the unsaturated soil in the direction of the gravitational acceleration; $D(\theta_u)$ is the moisture diffusion coefficient of the soil, which can be calculated by the following Equations 7–9 (Chen and Zhang, 2020):

$$D(\theta_u) = \frac{k_{ui}}{C(\theta_u)}, \tag{7}$$

where $C(\theta_u)$ is the specific water capacity (1/m); k_{ui} is the permeability coefficient of salinized frozen soil. This paper adopts the method of calculating the specific water capacity from the Van Genuchten (VG) model:

$$S_e = \frac{\theta - \theta_r}{\theta_s - \theta_r} = \frac{1}{[1 + (\alpha h_m)^n]^m}, \tag{8}$$

$$C(\theta_u) = a_0 m/(1-m) S_e^{\frac{1}{m}} \left(1 - S_e^{\frac{1}{m}}\right)^m, \tag{9}$$

where S_e is the relative saturation of frozen soil, θ_s is the saturated water content of the soil, and θ_r is the residual water content of the soil.

The permeability coefficient of salinized frozen soil k_{ui} is closely related to the pore diameter in the soil, with the pores in the soil being simplified as capillary tubes with different diameters.

As the temperature decreases, the solubility of salt in solution decreases, leading to the crystallization and precipitation of salt. The relationship between the volume fraction of crystallized salt and the volume fraction of unfrozen water, as well as the solution concentration, is established (Huang et al., 2008) as follows (Equation 10):

$$\theta_c = \begin{cases} \dfrac{[C - n(T)]\theta_u M_c}{\rho_c} & C \geq n(T) \\ 0 \quad C < n(T), \end{cases} \tag{10}$$

where n(T) is the solubility curve of easily soluble salts in the pores of the soil, which is a function of temperature.

If it is assumed that the salt solution is contained in a capillary tube with a radius of Ri (i = 1 − n), the solution is always saturated after the salt precipitation. If the supersaturation of the solution is not taken into account, the following Equation 11 is obtained:

$$C' = \begin{cases} n(T) & C > n(T) \\ C & C \leq n(T), \end{cases} \tag{11}$$

where C is the initial mass concentration of solution, C′ is the subsequent mass concentration of solution after cooling, Ri is the initial pore radius, and R_i' is the subsequent pore radius after the salt precipitation due to cooling. Assuming that the salt crystals are evenly deposited on the pore walls after salt precipitation, the quantity of salt crystallization equals the amount of variation in the pore (Equation 12):

$$\frac{M_c}{M\rho_c}\left(\pi R_{iu}^2 \frac{C}{100 - C} - \pi R_i^2 \frac{C'}{100 - C'}\right) = \pi R_{iu}^2 - \pi R_i^2, \tag{12}$$

where M_c is the molecular weight of salt after crystallization, M is the molecular weight of salt, and ρ_c is the specific gravity of the crystalline salt. For the same salt, $\frac{M_c}{M\rho_c}$ is a constant value. Let $\frac{M_c}{M\rho_c} = \alpha$, then Equations 12, 13 can be used to determine the pore radius R_i after salt precipitation (Bai et al., 2015):

$$R_i = R_{iu}\sqrt{\frac{[\alpha C - (100 - C)](100 - C')}{[\alpha C' - (100 - C')](100 - C)}}. \tag{13}$$

The following equation can be used to determine the connection between temperature T and pore radius R_i (Peng et al., 2021; Wang et al., 2019) as Equation 14:

$$R_i = \frac{\sigma_{ls}}{\rho_i L_f} \frac{T_i}{T_i - T}, \tag{14}$$

where Lf is the latent heat of ice melting, Lf = 3.34 × 105 J/Kg; Ti is the freezing temperature of saline soil; T is the temperature of saline soil; σ_{ls} is the ice water interface energy, where $\sigma_{ls} = 2.90\times10^{-2}$ J/m^2.

Using the unfrozen water characteristic curve, assuming the temperature range (T0, Tn) is divided into n equal parts, for every decrease of △θu in the unfrozen water content, the corresponding k increases by 1. When k = 0, ks represents the permeability coefficient of saturated thawed soil under the same conditions as Equation 15.

$$k_s = \frac{\pi\xi}{8\mu(\infty)} \sum_{i=1}^{M} n_i R_i^4, \tag{15}$$

where μ∞ is the viscosity of volumetric water, which is a function of temperature (Thomas and Sansom, 1995) and can be represented as $\mu_\infty(T) = 0.6612(T - 229)^{-1.562}$; ξ is the ratio of the soil column length H to the actual path of water seepage L(ξ =L/H), $\xi_i = 1 + 0.41\ln(1/\theta_i)$ (Ishizaki et al., 1996); n_i is the number of pores with the same diameter; R_i is the diameter of unfrozen pores.

Therefore, the permeability coefficient of saturated salinized frozen soil is expressed as (Zhang and Guan, 2022) Equation 16

$$k_i = k_s \frac{\mu(\infty)}{\mu(d)} \left[\sum_{i=k+1}^{M} n_i\left(R_i^4 + 4R_i^3 l_{s,t}\right) / \sum_{i=1}^{M} n_i R_i^4\right], \tag{16}$$

where $\mu(d)$ is the effective viscosity. The unfrozen water content in frozen soil equals the sum of liquid water in each pore, which can be expressed as Equation 17

$$\theta_u = \pi \sum_{i=k+1}^{M} n_i R_i^2. \tag{17}$$

The number of pores with diameter R_i, denoted as n_i, can be calculated from the unfrozen water characteristic curve. k_u is the permeability (m/s) of unsaturated soil. In this paper, the calculation method of the permeability coefficient of unsaturated soil is adopted by the VG model in Equation 18:

$$k_u = k_s S_e^{0.5}\left[1 - \left(1 - S_e^{\frac{1}{m}}\right)^m\right]^2 = k_s A, \tag{18}$$

where m and n are the VG model fitting parameters, which vary for different types of soils.

Therefore, the permeability coefficient of unsaturated salinized frozen soil is expressed as Equation 19

$$k_{ui} = \frac{k_u}{A} \frac{\mu(\infty)}{\mu(d)} \left[\sum_{i=k+1}^{M} n_i\left(R_i^4 + 4R_i^3 l_{s,t}\right) / \sum_{i=1}^{M} n_i R_i^4\right]. \tag{19}$$

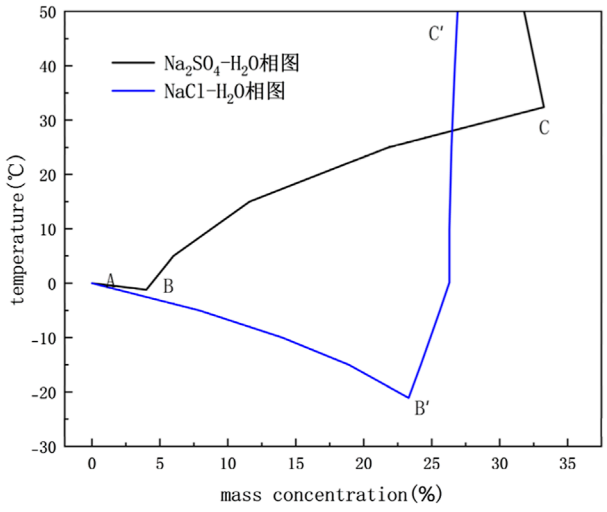

FIGURE 1
Phase diagram of the aqueous–salt binary system (Niu and Cheng, 2002).

2.3 Control equations for the salinity field

Convection, molecular diffusion, and mechanical dispersion are the main modes of salt transport in solutes. Amongst these modes, molecular diffusion and mechanical dispersion are collectively known as hydrodynamic dispersion (Jian et al., 2021; Ma et al., 2016).

Convection, which is the migration of salts along with water in the soil, has a significant effect on soil solute fluxes. The solute flux due to convection is related to the soil water flux and the concentration of the solution and can be described by the following Equation 20 (Ishizaki et al., 1996):

$$J_c = q_l C, \tag{20}$$

where J_c refers to the flux of solute due to convection through a unit area of soil in a unit of time, q_l is the flux of liquid water in the soil, and C is the solute concentration.

Molecular diffusion is the process of solute transport by ions or molecules due to Brownian motion (Wu et al., 2017; Xiao et al., 2015). This process is irreversible. It makes a solution in the presence of a concentration gradient, and the solution tends to be homogeneous. Molecular diffusion in soil pore solutions can also be described by Fick's first law as Equation 21:

$$J_d = -D_0 a e^{b\theta_u} \frac{\partial C}{\partial z}, \tag{21}$$

where J_d is the molecular diffusion flux of the solute, $\partial C/\partial z$ is the concentration gradient, D_0 is the molecular diffusion coefficient of solute in free water, e is the soil pore ratio, a and b are empirical parameters, a is generally taken between 0.005 and 0.001, and b is generally taken as 10.

Mechanical dispersion is due to the non-homogeneity of the soil. Therefore, the water flow in the soil pores has different magnitudes and directions, and the solute spreads to other ranges. The solute flux due to mechanical dispersion can be approximated by Fick's law as Equation 22 (Deng, 2006):

$$J_h = -\alpha |v| \frac{\partial C}{\partial z}, \tag{22}$$

where J_h is the solute flux due to mechanical dispersion, α is an empirical coefficient and is related to the nature of the soil itself, taking the value of 0.2–0.55 cm; $v = q/\theta$, q can be obtained from Darcy's law, $q = D\, d\theta/dy$.

The solute hydrodynamic dispersion effect can be described by the following Equation 23:

$$J_D = J_d + J_h = -\left[D_0 a e^{b\theta_u} + \alpha |v|\right] \frac{\partial C}{\partial z}, \tag{23}$$

where the total salt content comprises the readily soluble salt content in unfrozen water, the crystalline salt precipitated by ice crystallization, and the crystalline salt after solubility reduction as Equation 24:

$$\theta_w c = \theta_u c + \frac{\rho_i}{\rho_w}\theta_i c + \frac{\rho_c}{M_c}\theta_c. \tag{24}$$

Therefore, the salt field control (Equation 25) is (Liu et al., 2021; Zhao and Luo, 2019)

$$\frac{\partial\left(\boldsymbol{\theta_u c} + \frac{\rho_i}{\rho_w}\boldsymbol{\theta_i c} + \frac{\rho_c}{M_c}\boldsymbol{\theta_c}\right)}{\partial t} = \nabla\left[\boldsymbol{D_0 a e^{b\theta_u}} + \boldsymbol{\alpha |v|}\frac{\partial \boldsymbol{c}}{\partial z} + \boldsymbol{qc}\right]. \tag{25}$$

3 Model validation

3.1 Coupled hydrothermal salt numerical model

The results of the model calculations of sulfate and chloride saline soils under open conditions were compared with the experimental results to verify the validity and feasibility of the above numerical coupled hydrothermal salt model. During the temperature drop process of the soil sample, the unfrozen water content is determined by Formula 17, the freezing temperature T_i of the salinized soil, and the crystallization of salt is obtained from the water–salt (Na_2SO_4, NaCl) binary phase diagram. As shown in Figure 1, the freezing temperature T_i curves of saline soil are AB(Na_2SO_4) and AB′(NaCl), and the solubility curves of salt n(T) are BC(Na_2SO_4) and BC′(NaCl). These two curves intersect at the eutectic point B (Niu and Cheng, 2002). When the soil temperature drops to T_X, the corresponding amount of unfrozen water content, the freezing temperature, and salt crystallization are calculated from the relationship.

A numerical simulation of water–salt (Na_2SO_4, NaCl) migration in a one-way freezing test with brine recharge is conducted to analyze the water–salt migration and salt crystallization law of saline soil. Through the relevant model parameters, the model is set to be solved with the same initial and boundary conditions as the indoor test, and the numerical simulation results are compared with the measured data of the test to verify model validity.

Both salt crystallization and ice occur during the cooling process of Na_2SO_4 saline soil. However, in the calculation of NaCl saline soil, the concentrations of NaCl solution are preset to be 0.4 mol/kg, 0.6 mol/kg, 0.8 mol/kg, and 1.0 mol/kg, with NaCl contents in the

10.3389/feart.2024.1367771

TABLE 1 Basic soil parameters.

Parametric	Unit (of measure)	Retrieved value	Hidden meaning
ρ_w	$[kg/m^3]$	1,000	Density of water
ρ_i	$[kg/m^3]$	918	Density of ice
ρ_c	$[kg/m^3]$	1,460	Glauber's salt density
ρ_s	$[kg/m^3]$	2,700	Soil particle density
C_w	$[kJ/(m^3 \cdot K)]$	4.18	Specific heat capacity of water
C_i	$[kJ/(m^3 \cdot K)]$	2.09	Specific heat capacity of ice
C_c	$[kJ/(m^3 \cdot K)]$	1.74	Specific heat capacity of mannite
C_s	$[kJ/(m^3 \cdot K)]$	0.85	Specific heat capacity of earth particles
λ_w	$[W/(m \cdot K)]$	0.58	Thermal conductivity of water
λ_i	$[W/(m \cdot K)]$	2.22	Thermal conductivity of ice
λ_c	$[W/(m \cdot K)]$	1.35	Thermal conductivity of manganese
λ_s	$[W/(m \cdot K)]$	1.55	Thermal conductivity of soil particles
L_i	[kJ/kg]	334.56	Latent heat of phase transition of ice and water
L_c	[kJ/kg]	210	Latent heat of phase change of sodium sulfate crystallization
a_0	m^{-1}	2.59	VG model parameters
M	1	0.22	VG model parameters
L	1	0.50	VG model parameters
θ_s	1	0.36	Saturated moisture content
θ_r	1	0.02	Residual moisture content
k_s	[m/s]	10^{-8}	Saturated permeability coefficient
B	1	0.56	Solid–liquid ratio parameters
T_f	°C	−0.76	Freezing temperatures
A	M	0.3	Salinity parameter
D_0	$[m^2/h]$	0.31	Salinity parameter
B	1	10	Salinity parameter
a	1	2.61×10^{-4}	Salinity parameter
$Na_2SO_4 \cdot 10H_2O$	°C	−1.2	Eutectic temperature
	(%)	4	Eutectic concentration
		322.22	Molecular weight
	1	1.48	Specific gravity
$NaCl \cdot 2H_2O$	°C	−21.1	Eutectic temperature
	(%)	23.3	Eutectic concentration
		1.48	Molecular weight
	1	76.44	Specific gravity

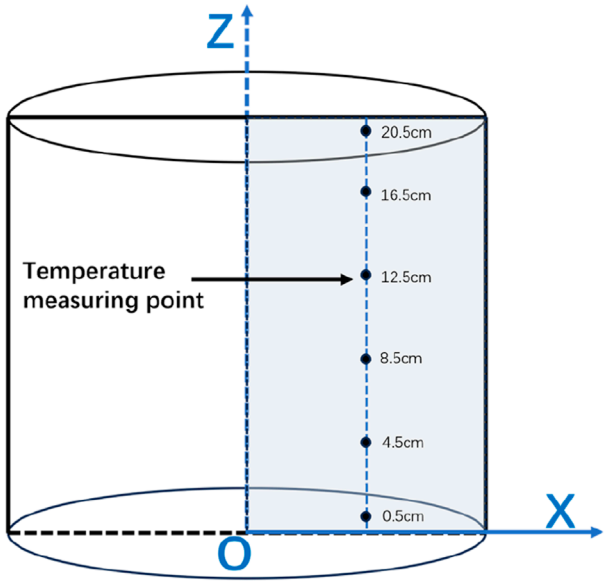

FIGURE 2
Geometric model for numerical computation.

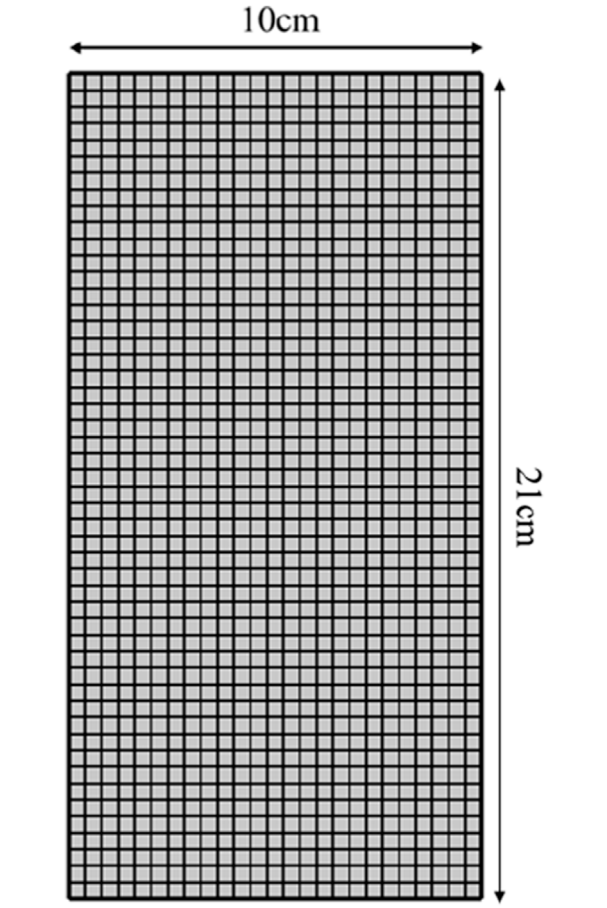

FIGURE 3
Finite element model meshing.

TABLE 2 Initial and boundary conditions in model calculation.

	Initial condition	Boundary condition
T	$T(t=0,x)=25°C$	$T(t,x=0)=-8°C$
		$T(t,x=0.21)=4°C$
θ	$\theta_w(t=0,x)=0.21$	$\theta_w(t,x=0)=0$
		$\theta_w(t,x=0.21)=0.21$
C	$C(t=0,x)=0.6$ mol/kg	$C(t,x=0)=0$
		$C(t,x=0.21)=0.6$ mol/kg

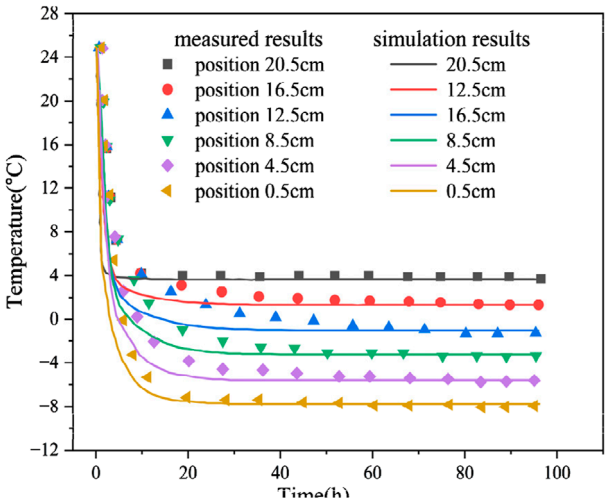

FIGURE 4
Temperature field distribution in the freezing test.

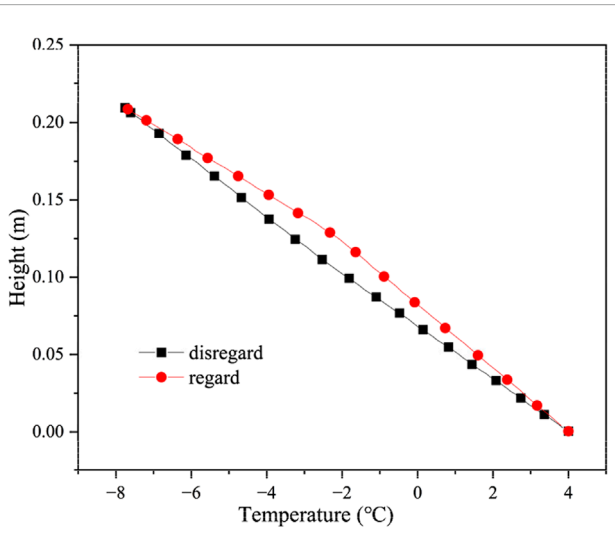

FIGURE 5
Temperature distribution of soil regarding and disregarding the latent heat of moisture phase change.

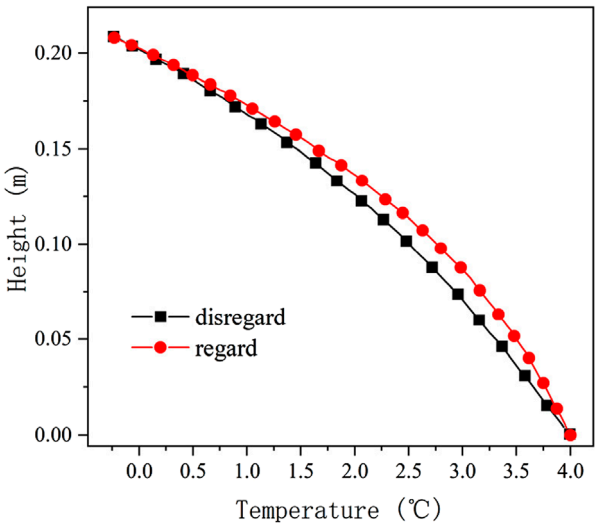

FIGURE 6
Temperature distribution of soil regarding and disregarding the latent heat of salt crystallization.

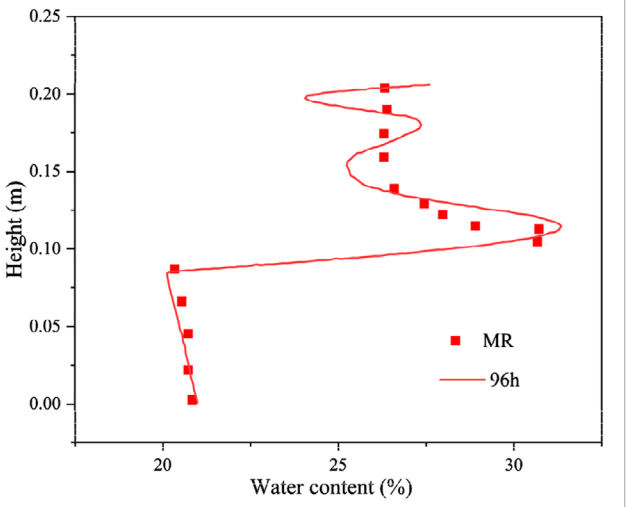

FIGURE 7
Distribution of water content in freezing tests.

soil of 0.412%, 0.618%, 0.824%, and 1.030%, respectively. The temperature ranges from −8°C to 4°C. As indicated by Figure 1, the NaCl-H_2O phase diagram, during the soil cooling process, NaCl does not crystallize; the NaCl content mainly affects the freezing temperature and the unfrozen water content of the soil. Therefore, neglecting NaCl crystallization, the influence of NaCl content on the soil's thermal conductivity, latent heat, and the pore diameter of phase transition is disregarded.

These soil parameters (Xu et al., 2021; Zhang et al., 2021b; Tang et al., 2023; Wan et al., 2015) are used for the model calculations (Table 1).

The model assumes the following:

1. The pores are not deformed, and the porosity remains constant;

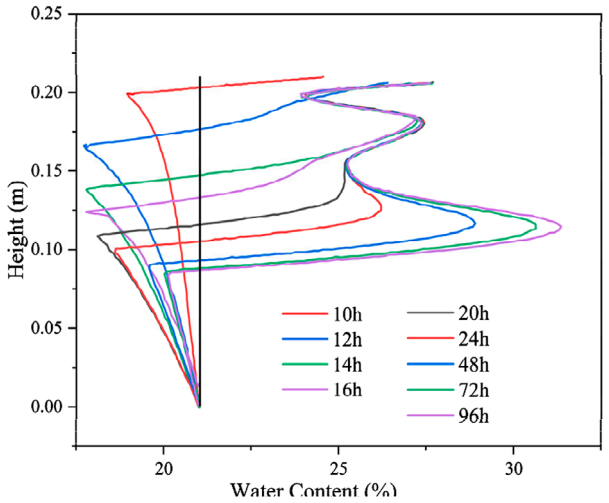

FIGURE 8
Distribution of water content at different moments in the freezing test.

2. The soil is not frozen at the initial moment;
3. The temperature, water content, and solute concentration of the specimen are uniformly distributed.

COMSOL was used to simulate the 2D frozen soil columns using a map illustration of a sub-grid with 1,200 cells, 148 boundary cells, and four vertex cells (Figures 2, 3). The model calculation time is 96 h, the calculation result output step is 1, and the solver step is set to intermediate.

3.2 Numerical simulation validation

To verify the accuracy of the model, it was configured with the same initial conditions and boundary conditions as the test (Zhang, 2020). Under water replenishment conditions, numerical simulations of unidirectional freezing of Na_2SO_4 saline soil were conducted, and the computed results were compared with test data. The variables of the equation, the boundary conditions, and the initial conditions set are shown in Table 2.

3.2.1 Temperature field result analysis

The numerical simulation temperature field distribution results in the freezing test are consistent with the measured results (MR) of the test (Figure 4). The trends of the temperature curves at different locations are more or less the same, and the temperature change displays stage characteristics: rapid cooling, slow cooling, and stabilization stages. In the rapid cooling stage, the temperature at each location of the soil column rapidly decreases; the temperature rapidly decreases when it is close to the boundary of the cold end. In the slow cooling phase, the required time for slow cooling at various locations is different, whilst the time required for the slow cooling phase is short when it is close to the cold-end temperature boundary. After 20 h of cooling, the internal temperature reaches the stabilization stage, and the temperature generally displays some fluctuations. Meanwhile, the difference between the calculated and test results for the freezing time of 10–20 h is substantial because

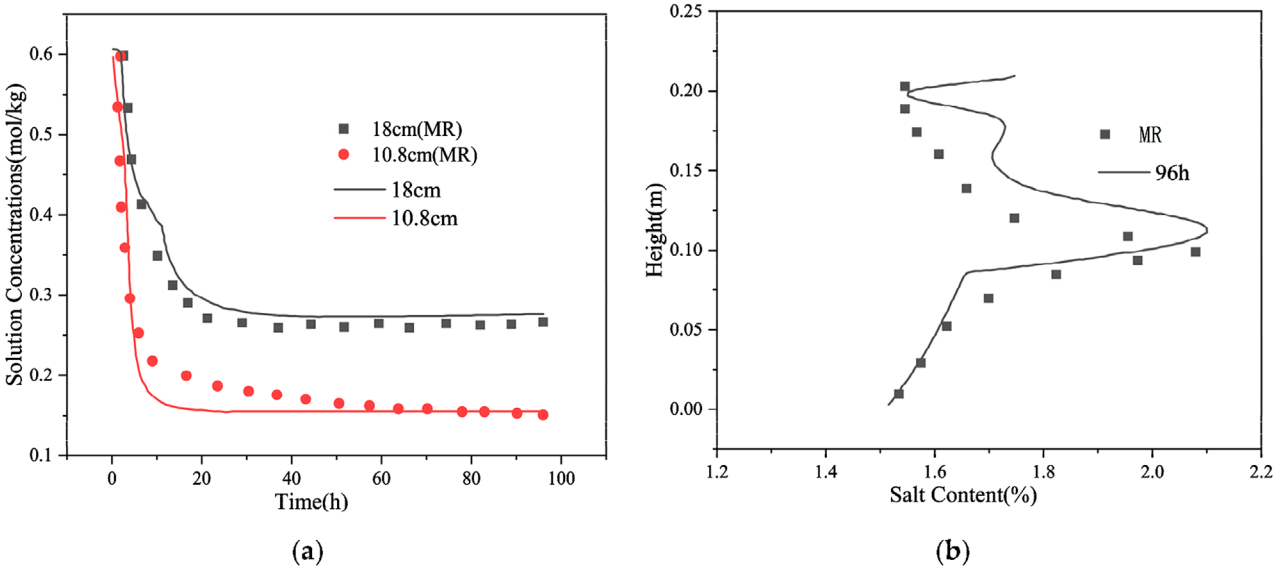

FIGURE 9
Distribution of solution concentrations and salt content in the freezing test. **(A)** Distribution of solution concentrations in the freezing test; **(B)** Salt content along depth distribution in the freezing tests.

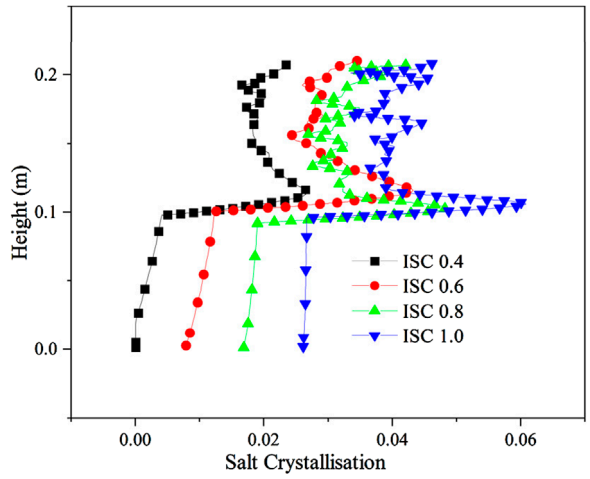

FIGURE 10
Distribution of salt crystallization volume for different initial solution concentrations.

the calculated results are all based on ideal conditions. The porosity may change in the freezing process, the water and salt contents of the specimen may not be uniformly distributed along the height direction, and the external temperature has a certain effect on the sidewall of the soil column.

Temperature distribution of soil regarding and disregarding the latent heat of moisture phase change is shown in Figure 5, the initial salt concentration of the soil is 0.6 mol/kg and the water content is 20%, respectively. The maximum temperature difference in the middle of the soil column, considering and disregarding the latent heat of moisture phase change, is 1.22°C. The migration of moisture from the unfrozen to the frozen zone will release heat due to the liquid-to-solid transition and the existence of a temperature gradient, which has a delaying effect on the soil temperature reduction.

The effect of salt phase transition on temperature for a saline soil with an initial solution concentration of 0.6 mol/kg and a soil salt content of 1.5% sulfuric acid is shown in Figure 6. When the boundary conditions, soil condition, and initial water content are the same, the maximum temperature difference in the soil is only 0.253°C when considering and disregarding the latent heat of crystallization of sodium sulfate. Which is a relatively smaller effect on the temperature gradient compared with the moisture phase change. This phenomenon is mainly due to the lesser amount of latent heat released by the crystalline salt with the same volume content as ice crystals and the smaller salt content of the soil compared to the water content.

3.2.2 Moisture field analysis of results

The numerical simulation results of the freezing test are consistent with the measured test results (Figure 7). These results are further compared to determine the consistency of the total volumetric water content test results and the calculation results in the lower part of the soil column. Meanwhile, the total volumetric water content calculation results oscillate in the upper part of the specimen, which is only partially in agreement with the test results. This finding is mainly due to the total volume water content measurement method, which aims to cut the specimen in layers and then use the drying method to measure the distribution of the total volume of water content along the height of the specimen, resulting in insufficiently precise test results.

The calculated results of the distribution of the total volumetric water content of the soil column along the specimen height at different moments are shown in Figure 8. The total volumetric

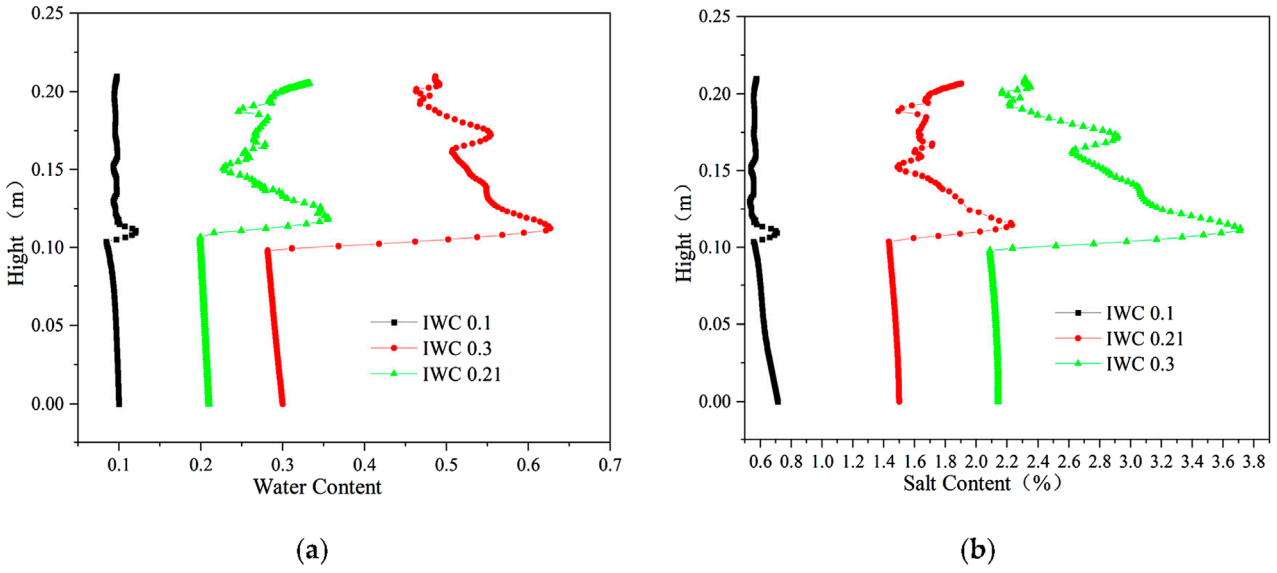

FIGURE 11
Distribution of aqueous salt along the specimen height after freezing for 96 h with different initial water contents. **(A)** Water content. **(B)** Salt content (Na_2SO_4).

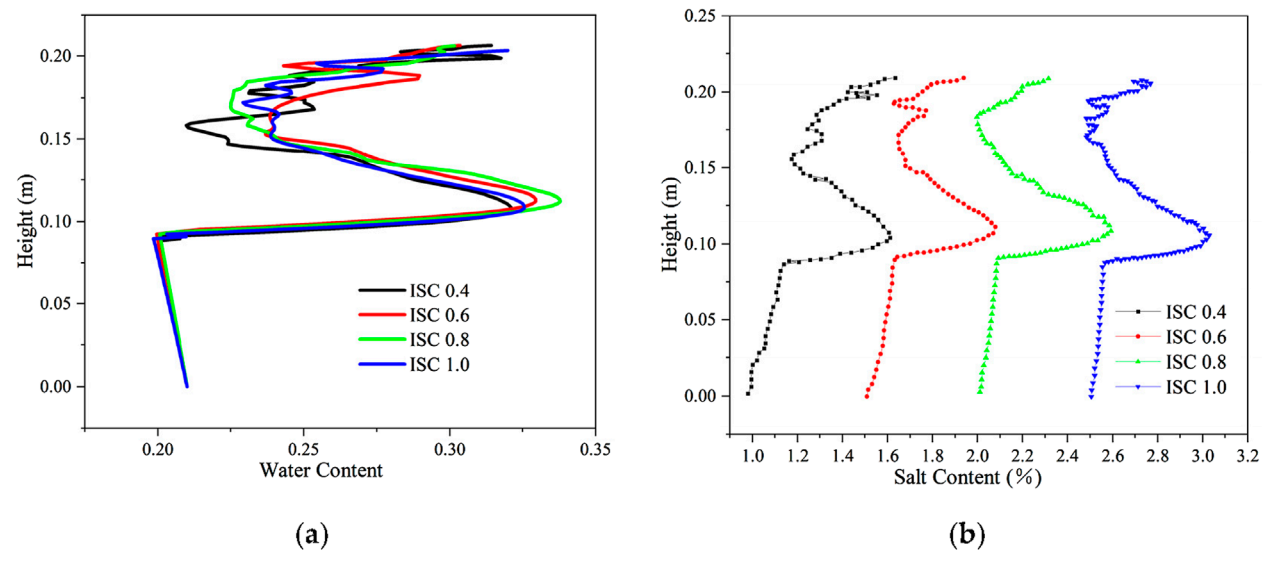

FIGURE 12
Distribution of aqueous salt along the specimen height after freezing for 96 h with different initial salt concentrations. **(A)** Water content. **(B)** Salt content.

water content in the unfrozen zone is always maintained at a constant value because of the recharge water at the bottom. After soil freezing, the water migrated upward, and a significant redistribution of the internal water occurred. This redistribution is attributed to moisture crystallization in the process of temperature reduction, forming a negative pressure head that draws moisture upwards. Simultaneously, as multiple freezing fronts are formed during the freezing process of the soil column, moisture aggregation occurs at several different locations, and the total volumetric water content is distributed along the specimen height oscillations. The maximum total volumetric water content distribution is also observed at the last formed freezing fronts with time, and the total volumetric water content is increased by approximately 52%.

3.2.3 Salt field analysis of results

The distribution results of solution concentration in the numerical simulation in the freezing test are consistent with the test results (Figure 9A). The upper soil has a low temperature and solution concentration after reaching stability, and the lower soil has a high temperature and solution concentration after reaching

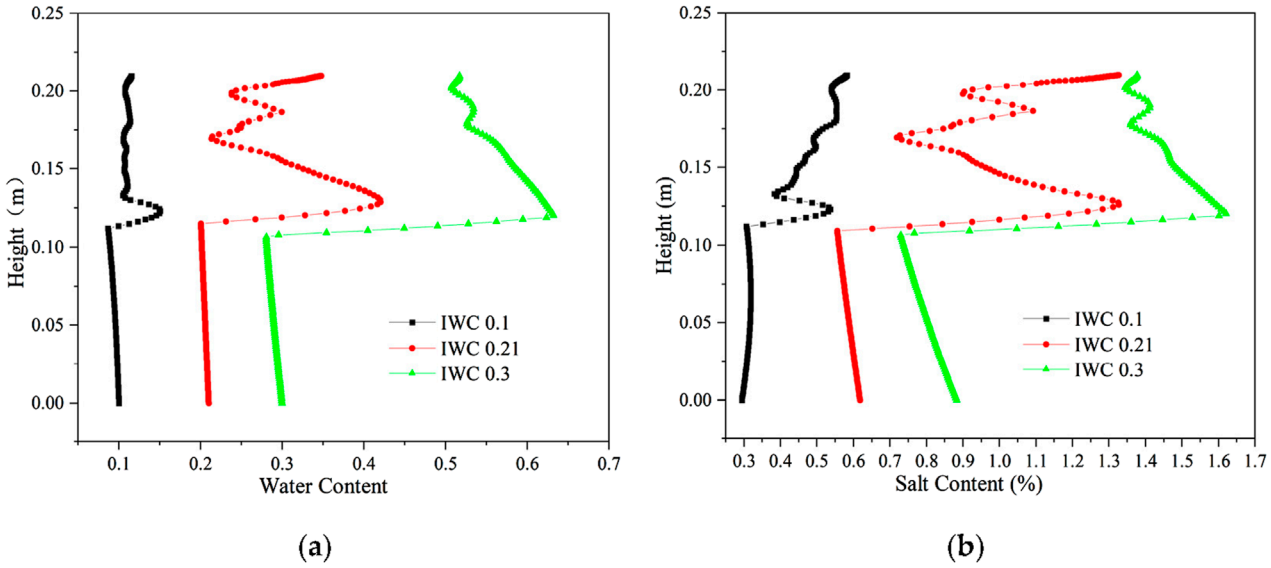

FIGURE 13
Distribution of aqueous salt along the specimen height after freezing for 96 h with different initial water contents. **(A)** Water content. **(B)** Salt content (NaCl).

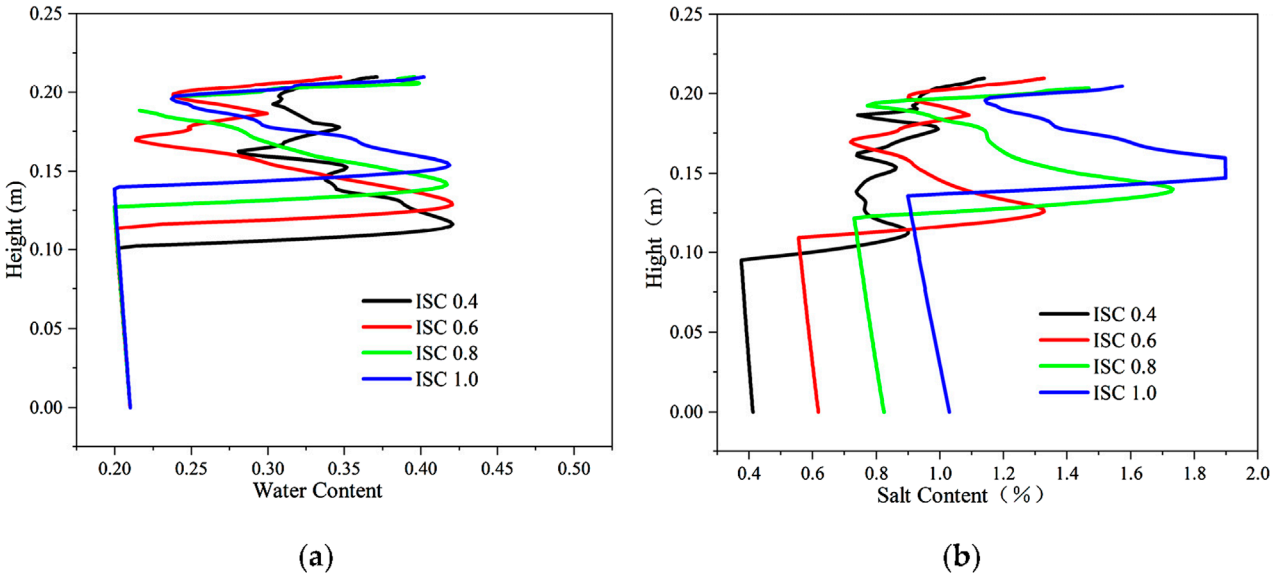

FIGURE 14
Distribution of aqueous salt along the specimen height after freezing for 96 h with different initial salt concentrations. **(A)** Water content. **(B)** Salt content (NaCl).

stability. At the freezing of the soil, the calculated results are in good agreement with the test results; at the freezing front, a certain difference is observed between the calculated and test results, which may be due to the intense water–salt migration at the freezing front as well as the salt–ice crystallization. The numerical simulation results of the salt content distribution after 96 h of freezing are consistent with the experimental results (Figure 9B). In the lower part of the soil, only the salts undergo a phase change, and the moisture does not undergo a phase change. Therefore, the calculation model is more in line with the actual situation, and the calculation results are in good agreement with the test results. In the upper part of the soil, a certain difference exists between the calculation and test results because the moisture and salt will undergo phase changes, thereby influencing and restraining each other, and the change in moisture and salt is remarkably complicated. The salt phase change process generally includes four stages: subcooling, jumping, constant, and decreasing stages. Meanwhile, the calculation model simplifies the process of salt

precipitation after freezing of the soil. At high temperatures, the salt will be precipitated as long as the solution concentration is greater than the solution degree; at low temperatures, the salt is precipitated in a substantially short time under the action of ice self-purification and precipitate crystals. Simultaneously, the model disregards the supersaturation of the solution; the salt will precipitate as long as the solution concentration is less than the solution degree, which is relatively different from the actual situation.

4 Results and discussion

The model was used to calculate the freezing behavior of Na_2SO_4 and NaCl saline soils with water replenishment on the bottom surface under different conditions. In the Na_2SO_4 saline soil, the initial salt concentration is 0.4 mol/kg, 0.6 mol/kg, 0.8 mol/kg, and 1.0 mol/kg; the salt content of the soil is 1%, 1.5%, 2%, and 2.5%, respectively.

In the NaCl saline soil, the initial salt concentrations were all 0.6 mol/kg, the initial volumetric water contents were 0.1, 0.21, and 0.3, and the salt content of the soil was divided into 0.294%, 0.618%, and 0.883%, respectively.

4.1 Water–salt migration patterns in sulfate-salted soils

The distribution of salt crystallization amount with different initial Na_2SO_4 concentrations is shown in Figure 10. According to the theoretical calculation model of freezing temperature, the freezing temperature of Na_2SO_4 soil comprises two parts: moisture activity and pore water freezing temperature. When the pore water freezing temperature of the sample is −0.76°C, the freezing temperature of the soil is −2.35°C, −2.5°C, −2.01°C and −2.22°C; at this time, the maximum crystalline amount of the salts is 0.263, 0.428 and 0.483. The maximum crystallization amount of salt is 0.263, 0.428, 0.483, and 0.6, and the salt crystallization amount is large under high initial salt content.

Due to the high initial temperature and large initial salt concentration, the salt crystallized in the upper and lower parts of the soil, and the upper part crystallized more than the lower part of the soil due to the low temperature. As the freezing temperature shows a decreasing, increasing, and then decreasing trend, the location of salt crystallization aggregation displays an increasing, decreasing, and then increasing trend, and the impact on the upper part of the sample is substantial when the location of salt crystallization is high.

The distribution of aqueous salt with different initial water contents (IWC) is shown in Figure 11. When the initial salt concentrations were all 0.6 mol/kg, the initial volumetric water contents were 0.1, 0.21, and 0.3, and the soil salt contents were 0.714%, 1.500%, and 2.143%, respectively. Thus, the freezing temperatures were all approximately −2.5°C. Due to similar initial salt concentrations, the soil freezing temperature is the same under different initial water contents, the location of the soil freezing front is consistent, and the locations of moisture salt migration and aggregation are also the same. The latent heat of moisture phase change has a certain delaying effect on cooling. Thus, the migration time of moisture and salt upward becomes longer when the water content is large, and the location of moisture and salt aggregation is slightly higher.

The distribution of aqueous salt with different initial salt concentrations is shown in Figure 12. When the salt concentration is 0.4 mol/kg, 0.6 mol/kg, 0.8 mol/kg, and 1.0 mol/kg, the initial volumetric water content is 0.21, the salt content of the soil is 1%, 1.5%, 2%, and 2.5%, respectively, and the freezing temperatures of soil are −2.35°C, −2.5°C, −2.01°C, and −2.22°C, respectively. As the salt concentration increases, the soil freezing temperature initially decreases, increases, and then decreases again, and the soil freezing front initially rises, falls, and then rises (2.01°C, −2.22°C). Moreover, the figures indicate that as the soil freezing temperature decreases, increases, and then decreases again with the rise in salt concentration, the soil freezing front rises, decreases, and then rises again, and there is a tendency for the location of the water–salt migration and aggregation to rise, fall, and then rise again. However, the location of water–salt aggregation is the same due to the small difference in freezing temperature.

4.2 Water–salt migration patterns in chlorine saline soils

The distribution of aqueous salt with different initial water contents is shown in Figure 13. When the initial NaCl concentrations were all 0.6 mol/kg, and the initial volumetric water contents were 0.1, 0.21, and 0.3, the NaCl content of the soil was divided into 0.294%, 0.618%, and 0.883%, respectively, and the freezing temperatures were all approximately −2.99°C. Due to the same initial salt concentration, the soil freezing temperature remains consistent under different initial water contents, the location of the soil freezing front is the same, and the location of moisture salt migration and aggregation also remains the same. The latent heat of moisture phase change has a certain delaying effect on the cooling. When the water content is large, the migration time of moisture and salt upward lengthens, and the location of moisture and salt aggregation is slightly elevated.

The distribution of aqueous salt with different initial NaCl concentrations is shown in Figure 14. The initial volumetric water content is 0.21; the NaCl concentrations are 0.4 mol/kg, 0.6 mol/kg, 0.8 mol/kg, and 1.0 mol/kg; the soil salt contents are 0.412%, 0.618%, 0.824%, and 1.030%, respectively; the solution freezing temperatures are taken as −1.46°C, −2.23°C, −2.98°C, and −3.74°C, respectively, and the soil freezing temperatures are −2.22°C, −2.99°C, −3.74°C, and −4.74°C, respectively. With the increase in salt concentration, the soil freezing temperature gradually decreases, the soil freezing front gradually moves upward, and the location of water–salt aggregation steadily rises. Compared with sulfate-salted soil, the permeability coefficient is relatively larger due to the absence of salts blocking the pores, and the upward water–salt migration is high. When the freezing temperature is high, the aggregation of the water–salt position in the upper soil is high, and the water–salt displays an oscillatory distribution; when the freezing temperature is low, the aggregation position of water in the upper soil decreases.

5 Conclusion

This article establishes a coupled model of water, heat, and salt fields based on the capillary model and the unfrozen water characteristic curve. The calculation and experimental results were compared and analyzed, which verified the reliability of the hydrothermal–salt coupling model in analyzing the salinization frozen soil problem. The conclusions are:

1. Different initial moisture contents have minimal effects on the location of soil salt migration and aggregation. When the moisture content is high, the water–salt migrates upward for a long time due to the gradual temperature reduction, and the location of water–salt migration and aggregation is slightly elevated upward.
2. Different initial salt concentrations have a substantial effect on the soil water–salt migration aggregation position. When the concentration of sodium chloride increases, the location of the water–salt migration and aggregation gradually move upward. When the concentration of sodium sulfate increases, unlike chloride saline soils, the position of the freezing front fluctuates up and down over time.
3. Compared with the open system with lower recharge, the water–salt migration and aggregation are smaller in the closed condition and are reduced by 38% and 20%, respectively, and the water–salt content in the lower part gradually decreases with increased freezing time.

Data availability statement

The original contributions presented in the study are included in the article/supplementary material; further inquiries can be directed to the corresponding author.

Author contributions

DB: Methodology, Conceptualization, Writing–review and editing. ZZ: Funding acquisition, Project administration, Supervision, Writing–original draft. ZY: Data curation, Methodology, Investigation, Writing–review and editing. AZ: Writing–original draft. GL: Data curation, Investigation, Writing–original draft.

Funding

The author(s) declare that financial support was received for the research, authorship, and/or publication of this article. This research was funded by the Tianshan Talent Training Program (2023TSYCLJ0055) and the National Natural Science Foundation of China (52068066 and 52368052).

Conflict of interest

Author DB was employed by Gansu Zhonghai Security Technology Co., Ltd.

The remaining authors declare that the research was conducted in the absence of any commercial or financial relationships that could be construed as a potential conflict of interest.

Publisher's note

All claims expressed in this article are solely those of the authors and do not necessarily represent those of their affiliated organizations, or those of the publisher, the editors, and the reviewers. Any product that may be evaluated in this article, or claim that may be made by its manufacturer, is not guaranteed or endorsed by the publisher.

References

Andersland, O. B., Wiggert, D. C., and Davies, S. H. (1996). Hydraulic conductivity of frozen granular soils. *J. Environ. Eng.* 122, 212–216. doi:10.1061/(asce)0733-9372(1996)122:3(212)

Bai, Q., Li, X., and Tian, Y. (2015). Equations and numerical simulation for coupled water and heat transfer in frozen soil. *Chin. J. Geotech. Eng.* 37, 131–136.

Bing, H., He, P., and Zhang, Y. (2015). Cyclic freeze–thaw as a mechanism for water and salt migration in soil. *Environ. Earth Sci.* 74, 675–681. doi:10.1007/s12665-015-4072-9

Bing, H., and Ma, W. (2011). Experimental study on freezing point of saline soil. *J. Glaciol. Geocryol.* 33, 1106–1113.

Burt, T. P., and Williams, P. J. (1976). Hydraulic conductivity in frozen soils. *Earth Surf. Process.* 1, 349–360. doi:10.1002/esp.3290010404

Chai, M., Zhang, J., Zhang, H., Mu, Y., Sun, G., and Yin, Z. (2018). A method for calculating unfrozen water content of silty clay with consideration of freezing point. *Appl. Clay Sci.* 161, 474–481. doi:10.1016/j.clay.2018.05.015

Chen, L., and Zhang, X. (2020). A model for predicting the hydraulic conductivity of warm saturated frozen soil. *Build. Environ.* 179, 106939. doi:10.1016/j.buildenv.2020.106939

Davidson, J. M., Stone, L. R., Nielsen, D. R., and Larue, M. E. (1969). Field measurement and use of soil-water properties. *Water Resour. Res.* 5, 1312–1321. doi:10.1029/wr005i006p01312

Deng, Q., Liu, X., Zeng, C., He, X., Chen, F., and Zhang, S. (2021). A freezing-thawing damage characterization method for highway subgrade in seasonally frozen regions based on thermal-hydraulic-mechanical coupling model. *Sensors* 21, 6251. doi:10.3390/s21186251

Deng, Y. (2006). Experimental study of permeability coefficient of saline soils. *J. Glaciol. Geocryol.* 28, 772–775.

Gardner, W. R. (1958). Some steady-state solutions of the unsaturated moisture flow equation with application to evaporation from a water table. *Soil Sci.* 85, 228–232. doi:10.1097/00010694-195804000-00006

He, P., Xiong, M., Mu, Y., Dong, J., and Na, X. (2021). Experimental study on frost-heaving force development of Tibetan clay subjected to one-directional freezing in an open system. *Adv. Civ. Eng.* 2021, 1–13. doi:10.1155/2021/6626149

Huang, D.-M., Sendner, C., Horinek, D., Netz, R. R., and Bocquet, L. (2008). Water slippage versus contact angle: a quasiuniversal relationship. *Phys. Rev. Lett.* 101, 226101. doi:10.1103/physrevlett.101.226101

Ishizaki, T., Maruyama, M., Furukawa, Y., and Dash, J. (1996). Premelting of ice in porous silica glass. *J. Cryst. Growth.* 163, 455–460. doi:10.1016/0022-0248(95)00990-6

Jian, X., Lan, W., Ren, C., Zhou, X., Wang, S., and Yuan, J. (2021). Modeling of coupled transfer of water, heat and solute in saline loess considering sodium sulfate crystallization. *Cold Reg. Sci. Technol.* 189, 103335. doi:10.1016/j.coldregions.2021.103335

Lai, Y.-M., You, Z.-M., and Zhang, J. (2021). Constitutive models and salt migration mechanisms of saline frozen soil and the-state-of-the-practice countermeasures in cold regions. *Sci. Cold Air Reg.* 13, 1–17.

Liu, G., Zhang, Z., Cheng, Z., Hao, G., Hao, Y., and Fu, T. (2023). Study on the permeability coefficient model of salinized frozen soil based on unfrozen water content curve. *Front. Earth Sci.* 10, 1102748. doi:10.3389/feart.2022.1102748

Liu, J., Yang, P., and Yang, Z.-J. (2021). Water and salt migration mechanisms of saturated chloride clay during freeze-thaw in an open system. *Cold Reg. Sci. Tech.* 186, 103277. doi:10.1016/j.coldregions.2021.103277

Luo, C., Yu, Y., Zhang, J., Tao, J. y., Ou, Q. j., and Cui, W. h. (2023). Thermal-water-salt coupling process of unsaturated saline soil under unidirectional freezing. *J. Mt. Sci.* 20, 557–569. doi:10.1007/s11629-022-7652-7

Ma, M., Bing, H., and Li, G.-Y. (2016). Experimental research on unfrozen water content of sodium sulphate saline soil. *J. Glaciol. Geocryol.* 38, 963–969.

Ming, F., Pei, W., Zhang, M., and Chen, L. (2022). A hydraulic conductivity model of frozen soils with the consideration of water films. *Eur. J. Soil Sci.* 73, e13210. doi:10.1111/ejss.13210

Niu, D., and Cheng, F. (2002) Phase diagrams of aqueous salt systems and their applications. M. *Phase diagrams of aqueous salt systems and their applications*.

Niu, X., and Gao, J. (2015). Expression for volume change of sulphate saline soil considering salt expansion and frost heave. *Chin. J. Geotech. Eng.* 37, 755–760.

Peng, E. X., Hu, X. Y., Sheng, Y., Wu, J. C., Cao, W., Yang, Q., et al. (2023). Thermal effect of the accumulated water with different depths on permafrost subgrade in cold regions. *Adv. Clim. Change Res.* 14, 179–189. doi:10.1016/j.accre.2022.08.003

Peng, E. X., Sheng, Y., Hu, X. Y., Wu, J. C., and Cao, W. (2021). Thermal effect of thermokarst lake on the permafrost under embankment. *Adv. Clim. Change Res.* 12, 76–82. doi:10.1016/j.accre.2020.10.002

Spaans, E. J. A., and Baker, J. M. (1996). The soil freezing characteristic: its measurement and similarity to the soil moisture characteristic. *Soil Sci. Soc. Am. J.* 60, 13–19. doi:10.2136/sssaj1996.03615995006000010005x

Tang, Q., Chen, Y., Jia, R., Guo, W., Chen, W., Li, X., et al. (2023). Effect of clay type and content on the mechanical properties of clayey silt hydrate sediments. *J. Pet. Sci. Eng.* 220, 111203. doi:10.1016/j.petrol.2022.111203

Thomas, H. R., and Sansom, M. R. (1995). Fully coupled analysis of heat, moisture, and air transfer in unsaturated soil. *J. Eng. Mech.* 121(3), 392–405.

Wan, X., Lai, Y., and Wang, C. (2015). Experimental study on the freezing temperatures of saline silty soils. *Permafr. Periglac. Process.* 26, 175–187. doi:10.1002/ppp.1837

Wang, D., Liu, J., and Li, X. (2016). Numerical simulation of coupled water and salt transfer in soil and a case study of the expansion of subgrade composed by saline soil. *Procedia Eng.* 143, 315–322. doi:10.1016/j.proeng.2016.06.040

Wang, X., Chen, R., Liu, G., Yang, Y., Song, Y., Liu, J., et al. (2019). Spatial distributions and temporal variations of the near-surface soil freeze state across China under climate change. *Glob. Planet. Change.* 172, 150–158. doi:10.1016/j.gloplacha.2018.09.016

Watanabe, K., and Flury, M. (2008). Capillary bundle model of hydraulic conductivity for frozen soil. *Water Resour. Res.* 44, 1–9. doi:10.1029/2008wr007012

Watanabe, K., and Osada, Y. (2016). Comparison of hydraulic conductivity in frozen saturated and unfrozen unsaturated soils. *Vadose Zone J.* 15, 1–7. doi:10.2136/vzj2015.11.0154

Wu, K., Chen, Z., Li, J., Li, X., Xu, J., and Dong, X. (2017). Wettability effect on nanoconfined water flow. *Proc. Natl. Acad. Sci. U.S.A.* 114, 3358–3363. doi:10.1073/pnas.1612608114

Xiao, B., Tu, X., Ren, W., and Wang, Z. (2015). Modeling for hydraulic permeability and Kozeny–Carman constant of porous nanofibers using a fractal approach. *Fractals* 23, 1550029. doi:10.1142/s0218348x15500292

Xiao, Z., and Lai, Y. (2018). Study on water and salt transfer mechanism in saline soil under freezing-thawing and dry-wet conditions. *Chin. J. Rock Mech. Eng.* 37, 3738–3746.

Xiao, Z., Lai, Y., and Zhang, M. (2018). Study on the freezing temperature of saline soil. *Acta Geotech.* 13, 195–205. doi:10.1007/s11440-017-0537-1

Xu, J., Lan, W., Ren, C., Zhou, X., Wang, S., and Yuan, J. (2021). Modeling of coupled transfer of water, heat and solute in saline loess considering sodium sulfate crystallization. *Cold Reg. Sci. Technol.* 189, 103335. doi:10.1016/j.coldregions.2021.103335

Zhang, H., Zhang, J.-M., Zhang, Z.-L., Andersland, O. B., Wiggert, D. C., and Davies, S. H. (2016). Measurement of hydraulic conductivity of Qinghai-Tibet Plateau silty clay under subfreezing temperatures. *Chin. J. Geotech. Eng.* 38, 1030–1035.

Zhang, J. (2020). *Study on the mechanism of water salt migration and crystallization deformation in sulfate saline soil in cold region*. Beijing, China: D. University of Chinese Academy of Science.

Zhang, S., Ye, S., and Zhang, L. (2020). Correction of hydrothermal salt force coupled equations for coarse-grained sulphate saline soil roadbed and its experimental verification. *J. Highw. Transp. Res. Dev.* 37, 31–40.

Zhang, X., Wu, Y., Zhai, E., and Ye, P. (2021a). Coupling analysis of the heat-water dynamics and frozen depth in a seasonally frozen zone. *J. Hydrol.* 593, 125603. doi:10.1016/j.jhydrol.2020.125603

Zhang, X., Zhai, E., Wu, Y., Sun, D., and Lu, Y. (2021b). Theoretical and numerical analyses on hydro–thermal–salt–mechanical interaction of unsaturated salinized soil subjected to typical unidirectional freezing process. *Int. J. Geomech.* 21, 04021104. doi:10.1061/(asce)gm.1943-5622.0002036

Zhang, Z., and Guan, C. (2022). *A model of hydraulic conductivity for frozen soil using unfrozen water content curve. J.* Journal of Xinjiang University, 039–004.

Zhao, J., and Luo, H. (2019). Transport and crystallization of NaCl solution in porous silicate materials. *J. Cryst. Growth.* 519, 25–34. doi:10.1016/j.jcrysgro.2019.05.003